Ann Surg Oncol (2019) 26:4587–4598
https://doi.org/10.1245/s10434-019-07910-x

Annals of
SURGICAL ONCOLOGY
OFFICIAL JOURNAL OF THE SOCIETY OF SURGICAL ONCOLOGY

ORIGINAL ARTICLE – HEPATOBILIARY TUMORS

Prediction of Histopathologic Growth Patterns of Colorectal Liver Metastases with a Noninvasive Imaging Method

Jin Cheng, MD[1], Jingwei Wei, PhD[2,3,4], Tong Tong, MD[5], Weiqi Sheng, MD[6], Yinli Zhang, MD[7], Yuqi Han, PhD[2,3,4], Dongsheng Gu, PhD[2,3,4], Nan Hong, MD[1], Yingjiang Ye, MD[8], Jie Tian, PhD[2,3,4,9,10], and Yi Wang, MD[1]

[1]Department of Radiology, Peking University People's Hospital, Beijing, China; [2]Key Laboratory of Molecular Imaging, Institute of Automation, Chinese Academy of Sciences, Beijing, China; [3]Beijing Key Laboratory of Molecular Imaging, Beijing, China; [4]University of Chinese Academy of Sciences, Beijing, China; [5]Department of Radiology, Department of Oncology, Fudan University Shanghai Cancer Center, Shanghai Medical College, Fudan University, Shanghai, China; [6]Department of Pathology, Department of Oncology, Fudan University Shanghai Cancer Center, Shanghai Medical College, Fudan University, Shanghai, China; [7]Department of Pathology, Peking University People's Hospital, Beijing, China; [8]Department of Gastrointestinal Surgery, Peking University People' Hospital, Beijing, China; [9]Beijing Advanced Innovation Center for Big Data-Based Precision Medicine, School of Medicine, Beihang University, Beijing, China; [10]Engineering Research Center of Molecular and Neuro Imaging of Ministry of Education, School of Life Science and Technology, Xidian University, Xi'an, Shaanxi, China

ABSTRACT

Objectives. To predict histopathologic growth patterns (HGPs) in colorectal liver metastases (CRLMs) with a noninvasive radiomics model.

Methods. Patients with chemotherapy-naive CRLMs who underwent abdominal contrast-enhanced multidetector CT (MDCT) followed by partial hepatectomy between January 2007 and January 2019 from two institutions were included in this retrospective study. Hematoxylin- and eosin-stained histopathologic sections of CRLMs were reviewed, with HGPs defined according to international consensus. Lesions were divided into training and validation datasets based on patients' sources. Radiomic features were extracted from pre- and post-contrast (arterial and portal venous) phase MDCT images, with review focusing on the segmented tumor–liver interface zones of CRLMs. Minimum redundancy maximum relevance and decision tree methods were used for radiomics modeling. Multivariable logistic regression analyses and ROC curves were used to assess the predictive performance of these models in predicting HGP types.

Results. A total of 126 CRLMs with histopathologic-demonstrated desmoplastic ($n = 68$) or replacement ($n = 58$) HGPs were assessed. The radiomics signature consisted of 20 features of each phase selected. The 3 phases fused radiomics signature demonstrated the best predictive performance in distinguishing between replacement and desmoplastic HGPs (AUCs of 0.926 and 0.939 in the training and external validation cohorts, respectively). The clinical-radiomics combined model showed good discrimination (C-indices of 0.941 and 0.833 in the training and external validation cohorts, respectively).

Conclusions. A radiomics model derived from MDCT images may effectively predict the HGP of CRLMs, thus providing a basis for prognostic stratification and therapeutic decision-making.

Jingwei Wei, Tong Tong and Weiqi Sheng have the equal contribution as the first authors.

Electronic supplementary material The online version of this article (https://doi.org/10.1245/s10434-019-07910-x) contains supplementary material, which is available to authorized users.

First Received: 22 June 2019;
Published Online: 11 October 2019

J. Tian, PhD
e-mail: tian@ieee.org

Y. Wang, MD
e-mail: wangyi@pkuph.edu.cn

In patients with colorectal cancer, the presence of liver metastases is a predictor of poor prognosis.[1,2] Liver resection confers the best prognosis for long-term survival in patients with colorectal liver metastases (CRLMs). Additionally, recent research has found that antiangiogenetic agent could improve the efficacy of cytotoxic chemotherapy, leading to improved overall survival.[3] For the initially unresectable CRLMs, the Bevacizumab-containing chemotherapy has been recommended as one of the regimens for the primary care and the continuum treatment, according to the NCCN guideline.[4] However, predicting and assessing the response to these therapies in patients with CRLMs is challenging, and inaccurately assessing response can lead to poor therapeutic decision-making, potentially affecting overall survival.

Because inter- and intra-tumor heterogeneity has been observed in patients with colorectal cancer, effective treatment may vary widely among patients. Therapeutic decision-making therefore must rely on tumor characterization in terms of genetic, epigenetic, phenotypic, and morphologic biomarkers. One such morphologic characteristic is the histopathologic growth pattern (HGP) of CRLMs. Liver metastases present with three major HGPs: desmoplastic, replacement, and pushing, and the first two types are most common.[5] In the desmoplastic HGP, the cancer cells are separated from the liver tissue by a rim of fibrous tissue with lymphocytic infiltration; sprouting angiogenesis also could be seen. In the replacement HGP, the cancer cells form cell plates that are in continuity with the liver cell plates, demonstrating co-option of sinusoidal blood vessels and the perisinusoidal space, as well as the trabecular architecture of the liver parenchyma are kept.[5–7] The metastatic vessels are continuous with the sinusoidal system of the liver, suggesting a mechanism of vascularization of vessel co-option.[8,9]

Because CRLMs with replacement HGP rely on vessel co-option instead of angiogenesis, these lesions respond more poorly than desmoplastic CRLMs to antiangiogenetic therapy.[10,11] Additionally, replacement CRLMs are associated with poorer overall survival than desmoplastic lesions, especially after the use of Bevacizumab.[6,10–13] Because of these differences, predictive biomarkers are needed to facilitate the use of tailor-made treatment strategies. However, HGPs of CRLMs are generally identified via histopathologic analysis of the entire resected CRLM specimen, thus limiting the clinical application.

Radiomics, an emerging technique, converts medical images into mineable data by extracting quantitative features, thus providing in-depth characterization of tumor phenotypes.[14,15] Radiomics analysis is complementary to biopsies but is noninvasive and allows evaluation of the whole lesion and microenvironment, characterization of spatial heterogeneity, and longitudinal assessment of disease progression.[15] Compared with conventional qualitative imaging feature analysis, radiomics analysis provides quantification of intra-tumor heterogeneity related to clinical issues through the use of machine learning methods.[16] This technique has been successfully used to assess genetic mutations, lymph node metastases, and therapy response prediction in patients with colorectal cancer.[17–19]

Because the different HGPs reflect various phenotypes of CRLMs, we assume that the type of HGP could be predicted with a radiomics approach using contrast-enhanced MDCT images.[20] Thus, we sought to construct a radiomics-based model by integrating both radiomic features and related clinical factors and we compared this model with conventional clinical/qualitative radiologic models in terms of each model's ability to predict HGPs in CRLMs before treatment.

MATERIALS AND METHODS

Study Population

This retrospective study was approved by the institutional review board (IRB) with a waiver of informed consent. Patients from two institutions were enrolled. A search of each hospital's histopathologic electronic information system (HIS) was performed to identify consecutive patients with CRLMs who had undergone contrast-enhanced MDCT followed by partial hepatectomy between January 2007 and January 2019. The exclusion criteria were as follows: (1) abdominal MDCT with contrast enhancement was not performed before surgery; (2) interval between abdominal MDCT and surgery was > 4 weeks; (3) neoadjuvant chemotherapy was administrated before hepatectomy; (4) MDCT images were not adequate for qualitative and quantitative analyses; and (5) hematoxylin- and eosin-stained (H&E) sections of the entire resected CRLM specimen were not available for analyses (Fig. 1).

Clinical characteristics were all recorded from HIS, which including patient's gender, age, occurrence time of the CRLMs (synchronous/metachronous), number of resected CRLM lesions per patient, time between CT scanning and surgery, and the location of primary cancer (rectum/colon).

MDCT Image Acquisition

Qualitative and quantitative analyses were performed on pre- and post-contrast (arterial and portal venous phase) images. Given the time span of the study, the images were

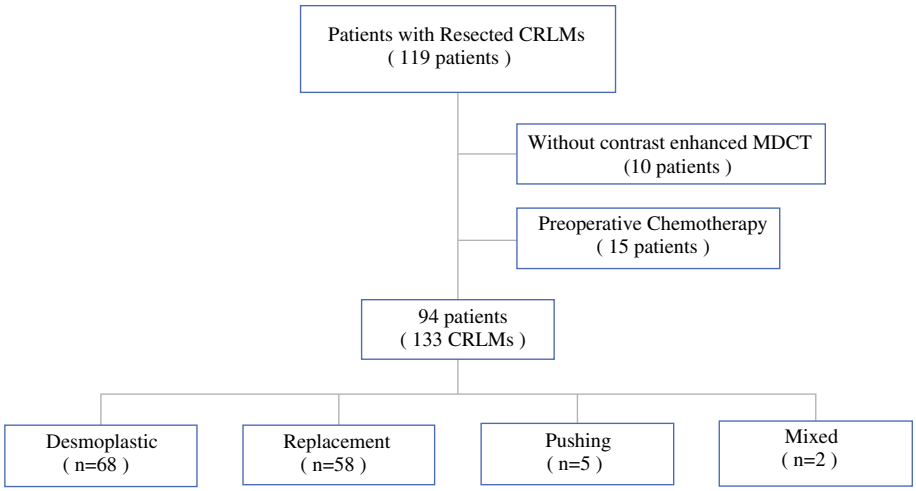

FIG. 1 Flow chart of patient enrollment

obtained on a variety of scanners; however, the scanning parameters (120 kV, 240–400 mA, slice thickness of 5 mm) and protocols for contrast agent use (100 mL Iopromide 370 mg/mL at a rate of 2.5 mL/s; Bayer Schering Pharma) were similar for all cases. MDCT scans in the arterial and portal venous phases were initiated at approximately 10 and 45 s, respectively, once the trigger threshold (100 HU on the abdominal aorta) had been reached.

Histopathologic Analysis

For each resected CRLM specimen, H&E-stained sections from ≥ 4 formalin-fixed paraffin-embedded blocks were retrospectively reviewed and categorized based on the international consensus guidelines for the definition of liver metastasis HGPs. Lesion for which $> 50\%$ of the TLI was identified as exhibiting one of the three HGPs was allocated to a group labelled as predominantly of this HGP (i.e., $> 50\%$ desmoplastic were categorized as predominantly desmoplastic HGP; $> 50\%$ pushing were categorized as predominantly pushing HGP; and $> 50\%$ replacement were categorized as predominantly replacement HGP).[13] For lesions exhibiting more than two HGPs and any HGP less than 50% was considered as mixed HGP. Histopathological type and tumor differentiation of CRLMs also were reviewed. Archived histologic material from each patient was retrospectively reviewed by two experienced hepatobiliary pathologists (W.Q.S. and Y.L.Z., with 15 and 10 years of experience, respectively) who were blinded to the clinical data. If the reviewers disagreed, they discussed the case until a consensus was met.

Qualitative Image Analysis

Two board-certified radiologists (J.C. and T.T., both with 10 years of experience in abdominal radiology) reviewed the MDCT images independently. Cases with a discrepancy in these subjective evaluations were jointly reviewed by the two readers until a consensus was met.

Tumor liver interface (TLI) was recorded as obscure or clear according to previously defined morphologic criteria.[21,22]

The readers also recorded the presence or absence of an enhanced rim on arterial phase (AP) and portal venous phase (PP) imaging. An enhanced rim on post-contrast imaging is typically seen with CRLMs, appearing as a ring with a density that is higher than that of the tumor or background liver.[23,24]

The location of the tumor (left or right lobe of the liver) also was recorded. The size of the tumor was recorded based on PP images, with the longest diameter of the tumor on the axial plane measured in millimeters.

Qualitative Imaging Model Construction

To determine whether qualitative imaging characteristics and quantitative radiomic features could be used for differentiation, we constructed a qualitative imaging model by integrating the five radiologic imaging characteristics (lesion location, size, TLI, enhanced rim on AP and P) using logistic regression modeling.

Clinical Model Construction

Five clinical characteristics (age, gender, occurrence time of the CRLMs, histopathological type and tumor differentiation of CRLMs, and location of primary cancer) were included in the clinical model. To determine the

predictive power of qualitative imaging and clinical factors, univariable analysis was initially used to select related qualitative imaging and clinical factors with P values < 0.1. Multivariable analysis was then performed to select the final predictive qualitative imaging and clinical factors with P values < 0.05. A clinical model incorporating the selected factors was then constructed using logistic regression modeling.

Radiomics Model Construction

Segmentation Quantitative image analysis was performed on pre- and post-contrast (arterial and portal venous phase) images of the index tumor. Because the HGPs were identified at the tumor periphery in liver metastases on histopathology, segmentations were performed on the TLI zone (subtracting the outer segmentation image from the inner segmentation image).[6] The TLI zone was measured histopathologically with a scale of approximately 0.5 mm, which is the mean thickness of the fibrous capsule in the desmoplastic pattern, and the maximum thickness is approximately 2 mm.[25] To cover the entire TLI zone and for the operability, we placed the outer ring approximately 2 mm out from the edge of the tumor and the inner ring approximately 2 mm within the edge of the CRLMs.

Quantitative Radiomic Feature Extraction In total, a set of 540 radiomic features were extracted from the segmented TLI zones in the original images and in 8 filtered images through wavelet transformation. There were two types of features: first-order features and textural features. First-order features described gray-level intensity distribution of the original images. Textural features described granular texture patterns from four textural matrixes: gray-level co-occurrence matrix, gray-level run-length matrix, gray-level size zone matrix, and neighborhood gray-tone difference matrix (supplemental Table 1). To test the reproducibility and stability of the extracted features, we calculated the intraclass and interclass correlation coefficients, respectively.

Radiomics Modeling The lesions were divided into training and validation for model construction and external validation, based on different institution, respectively. Radiomics modeling was divided into two phases: feature selection and classification modeling. To select most HGP-related features, minimum redundancy maximum relevance (MRMR) was used as the feature selection algorithm. This algorithm was used to select the set of features that could best characterize the difference between replacement and desmoplastic HGPs while ensuring that the features were mutually dissimilar from each other to the maximum extent. For differentiation between replacement and desmoplastic HGPs, we adopted a decision tree (DT) as the classifier. This method has been widely used in previous radiomics studies.[26–28] Three final radiomics signatures were derived from pre-contrast, arterial, and PP MDCT images.

Combined Model and Nomogram Construction

To explore whether qualitative imaging and clinical factors had additional power for predicting HGP differentiation, we combined selected clinical factors with a tree-based radiomics signature using logistic regression modeling. Additionally, a nomogram was constructed based on the extent that clinical factors and radiomic signature contributed to HGP differentiation.

Model Assessment

The predictive performance of each model was assessed with ROC curves. AUC, accuracy, specificity, and sensitivity were calculated as detailed indicators. The models were compared using a DeLong test. We used calibration curves (Hosmer–Lemeshow test) to determine the agreement between nomogram-predicted HGPs and the actual status of HGPs.[29] All model assessments were performed for both training and external validation datasets.

Statistical Analysis

Categorical variables were described as number (n) and percentage (%). The mean value ± standard deviation or the median with interquartile ranges was calculated for quantitative variables that were tested assuming an abnormal distribution. A t test was used to analyze the difference between continuous variables. A Pearson χ^2 test was used to analyze the difference between categorical variables. Statistical analysis was performed with PASW Statistics version 18.0 (SPSS Inc., Chicago, IL) for Windows (Microsoft Corporation, Redmond, WA) and R version 3.4.1.

RESULTS

Clinical and Histopathologic Characteristics

The final study cohort consisted of 94 patients, including 59 men (62.8%) and 35 women (37.2%), with a median age of 63 (interquartile range, 53–72) years. Twenty-six (27.7%) patients were with metachronous metastatic tumor. Among them, 17 (65.4%) patients underwent

adjuvant chemotherapy (FOLFOX regimen for 12 cycles or XELOX regimen for 6–8 cycles) after the resection of the primary tumor. The median interval between the diagnosis of liver metastases and the end of the chemotherapy was 5 (interquartile range, 3–7) months. The median interval between MDCT and surgery was 12.5 (interquartile range, 2–27) days.

Among these patients, 133 lesions had been treated with partial hepatectomy and were analyzed in this study. The average number of lesions per patient was 1.12 (range, 1–7); 20 patients had multiple CRLMs. Based on the international guidelines for scoring liver metastasis HGPs, 68 (51.1%) were desmoplastic HGPs (Fig. 2a), 58 lesions (43.6%) were replacement HGPs (Fig. 2d), 5 (3.8%) were pushing HGPs, and 2 (1.5%) were mixed HGPs.[13] Only one patient had CRLMs of both desmoplastic and replacement HGPs. Pushing and mixed HGPs were excluded from the final qualitative and quantitative analyses because of the small sample size.

Finally, 68 CRLMs with desmoplastic HGP and 58 with replacement HGP were analyzed by qualitative imaging characteristics and a radiomics approach. The lesions were divided into training (n = 96) and validation (n = 30) lesions for model construction and external validation, respectively. The baseline characteristic distributions of training and validation cohorts are shown in Table 1.

Predictive Performance of the Qualitative Imaging Model

All lesions demonstrated a round shape with a shallow lobular appearance (Fig. 2b–f). More desmoplastic HGP lesions demonstrated as clear TLI, as well as rim enhancement on AP and PP respectively, than did replacement HGP lesions (Table 1). Significant differences were obtained by univariable analysis, but only the last one was significant different by multivariable analysis (Table 2). The qualitative imaging model integrating radiologic imaging characteristics demonstrated potential power for HGP recognition, with AUCs of 0.774 and 0.649 in the training and external validation cohorts, respectively (Table 3; Fig. 3a, b).

Predictive Performance of the Clinical Model

Age, gender, and tumor differentiation were chosen as effective predictors of HGP after univariable and multivariable analyses (Table 2). The AUC of the clinical model, which was constructed by combining the clinical

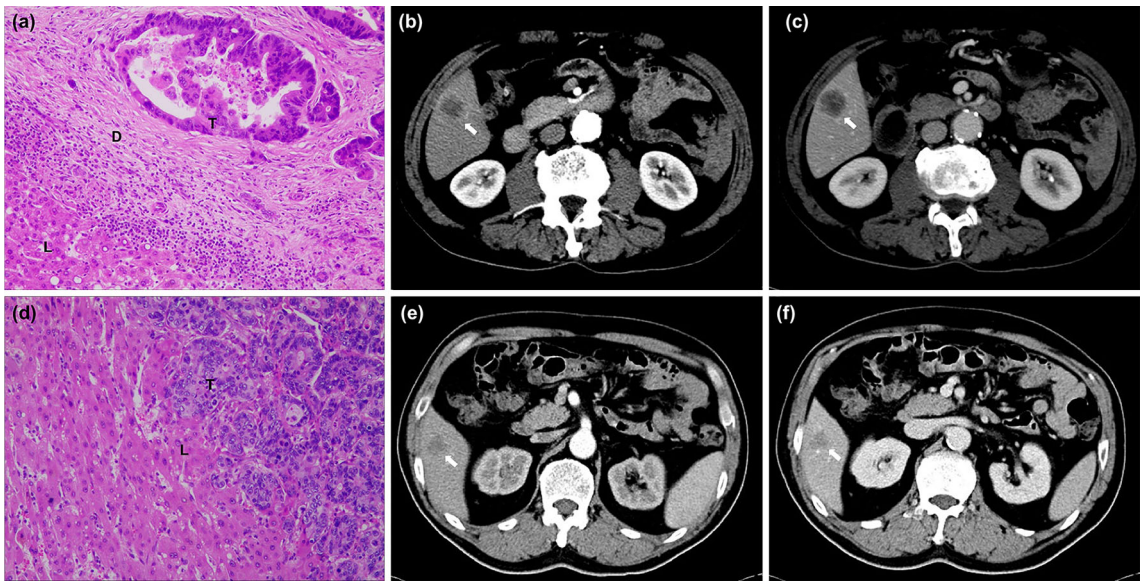

FIG. 2 H&E and MDCT images of different HGPs of CRLMs. **a** High magnification images of the desmoplastic growth pattern. MDCT images shew a desmoplastic CRLM (arrows) with clear tumor-liver interface (TLI) and rim enhancement on arterial **b** and portal venous **c** phases. **d** High magnification images of the replacement growth pattern. MDCT images shew a replacement CRLM (arrows) with obscure TLI and no rim enhancement on arterial **e** and portal venous phase **f**. T, tumor tissue; L, liver parenchyma; D, dense fibrous band

TABLE 1 Demographics among patients with training and validation cohorts of colorectal liver metastases

Models	Training dataset (n = 96)			Validation dataset (n = 30)			
	Desmoplastic (n = 55)	Replacement (n = 41)	P value	Desmoplastic (n = 13)	Replacement (n = 17)	P value	P value
Age (year)			0.383			0.697	0.140
≤ 63	30 (53.6%)	26 (46.4%)		10 (45.5%)	12 (54.5%)		
> 63	25 (62.5%)	15 (37.5%)		3 (37.5%)	5 (62.5)		
Gender			0.360			0.050	0.801
Female	23 (52.3%)	21 (47.7%)		3 (23.1%)	10 (76.9%)		
Male	32 (61.5%)	20 (38.5%)		10 (58.8%)	7 (41.2%)		
Primary cancer			0.923			0.977	0.105
Rectum	22 (57.9%)	16 (42.1%)		3 (42.9%)	4 (57.1%)		
Colon	33 (56.9%)	25 (43.1%)		10 (43.5%)	13 (56.5%)		
Synchronous			0.363			0.657	0.432
Yes	34 (54.0%)	29 (46.0%)		9 (40.9%)	13 (59.1%)		
No	21 (63.6%)	12 (36.4%)		4 (50.0%)	4 (50.0%)		
Lesion location			0.035			0.376	0.180
Left lobe	19 (45.2%)	23 (54.8%)		5 (55.6%)	4 (44.4%)		
Right lobe	36 (66.7%)	18 (33.3%)		8 (38.1%)	13 (75.0%)		
Size (longest diameter)			0.063			0.310	0.542
< 19.8 mm	23 (47.9%)	25 (52.1%)		6 (35.3%)	11 (64.7%)		
≥ 19.8 mm	32 (66.7%)	16 (33.3%)		7 (53.8%)	6 (46.2%)		
Tumor-liver interface			0.023			0.427	<0.001
Clear	33 (68.7%)	15 (31.3%)		12 (46.2%)	14 (53.8%)		
Obscure	22 (45.8%)	26 (54.2%)		1 (25%)	3 (75%)		
Enhanced rim on AP			< 0.001			0.469	0.454
Yes	29 (80.6%)	7 (19.4%)		2 (25.0%)	6 (66.7%)		
No	26 (43.3%)	34 (56.7%)		11 (50.0%)	11 (50.0%)		
Enhanced rim on PP			< 0.001			0.222	0.236
Yes	32 (86.5%)	5 (13.5%)		2 (25.0%)	6 (75.0%)		
No	23 (39.0%)	36 (61.0%)		11 (50.0%)	11 (50.5%)		
Differentiation			0.518			0.222	0.223
Poor	8 (50.0%)	8 (50.0%)		2 (25%)	6 (75.0%)		
Moderate	47 (58.8%)	33 (41.3%)		11 (50.0%)	11 (50.0%)		

factors and qualitative imaging factors, was 0.751 in the training cohort and 0.536 in the external validation cohort (Table 3; Fig. 3a, b). The accuracy value with this clinical model was 70.8% and 50.0% for the training and external validation datasets, respectively (Table 3).

Selected Features for Radiomics Signature Construction

Features were initially selected through an evaluation of robustness and reproducibility (Supplemental Fig. 1a–f). A total of 20 features were chosen for radiomics signature construction on AP and PP images obtained before and after contrast (Supplemental Table 2).

Predictive Performance of Tree-Based Radiomics Signatures

Three decision tree-based radiomics signatures were constructed by integrating the selected radiomic features on arterial and portal phase images obtained before and after contrast enhancement (Supplemental Fig. 2a–c). The fused radiomics signature (signature $^{pre+AP+PP}$) of three phases resulted the formula as following:

TABLE 2 Results of univariable and multivariable analyses in distinguishing replacement from desmoplastic histopathological growth pattern of colorectal liver metastases

Clinical predictor	Univariable analysis		Multivariable analysis	
	P value	OR (95% CI)	*P* value	OR (95% CI)
Age (yr)	0.754	0.994 (0.961–1.030)		
Gender	0.089	0.539 (0.265–1.098)	0.033	0.419 (0.188–0.933)
Lesion location	0.201	0.626 (0.306–1.282)		
Primary cancer	0.183	0.542 (0.220–1.334)		
Synchronous	0.274	1.526 (0.715–3.257)		
Differentiation	0.183	0.542 (0.220–1.334)		
Lesion size (longest diameter, mm)	0.031	0.454 (0.222–1.930)	0.577	0.789 (0.344–1.813)
Tumor–liver interface	0.032	0.450 (0.216–0.935)	0.755	0.866 (0.351–2.134)
Enhanced rim on arterial phase imaging	0.005	0.325 (0.149–0.709)	0.935	1.058 (0.276–4.048)
Enhanced rim on portal vein phase imaging	< 0.001	0.234 (0.104–0.526)	0.021	0.218 (0.060–0.94)

TABLE 3 Predictive performance in distinguishing replacement from desmoplastic histopathological growth pattern of colorectal liver metastases for the clinical, qualitative, radiomics, and combined models

Models	Training dataset (n = 96)				Validation dataset (n = 30)			
	AUC (95% CI)	Accuracy (%)	Sensitivity (%)	Specificity (%)	AUC (95% CI)	Accuracy (%)	Sensitivity (%)	Specificity (%)
Qualitative	0.774 (0.679–0.868)	71.9	82.9	63.6	0.649 (0.453–0.846)	66.7	82.4	46.2
Clinical	0.751 (0.658–0.843)	70.8	87.8	58.2	0.536 (0.340–0.733)	50.0	76.3	15.4
Radiomics								
Pre-contrast	0.739 (0.642–0.836)	68.8	73.2	65.5	0.758 (0.586–0.930)	70.0	82.4	53.8
Arterial phase	0.777 (0.642–0.845)	72.9	92.7	58.2	0.762 (0.616–0.909)	76.7	94.1	53.8
Portal phase	0.811 (0.748–0.875)	70.8	100.0	49.1	0.790 (0.653–0.926)	76.7	64.7	92.3
Pre + AP + PP	0.926 (0.875–0.978)	86.5	100.0	76.4	0.939 (0.859–1.000)	76.7	64.7	92.3
Combined								
Radiomics signature + clinical factors	0.941 (0.893–0.987)	88.5	100.0	80.0	0.833 (0.672–0.993)	73.3	58.8	92.3

$$\text{Radiomices signature} = \frac{\exp(-13.137 + 5.011 * \text{AP}_{\text{score}} + 10.268 * \text{PVP}_{\text{score}} + 2.307 * \text{NP}_{\text{socre}})}{1 + \exp(-13.137 + 5.011 * \text{AP}_{\text{score}} + 10.268 * \text{PVP}_{\text{score}} + 2.307 * \text{NP}_{\text{socre}})}.$$

The fused radiomics signature showed the best predictive performance in distinguishing between replacement and desmoplastic HGPs (Fig. 4a). The AUCs for signature $^{\text{pre+AP+PP}}$ in the training and external validation cohorts were 0.926 and 0.939, respectively ($P < 0.001$). Detailed performance indicators are shown in Table 3. The subsequent signatures involved PP (signature$^{\text{PP}}$), AP (signature$^{\text{AP}}$), and pre-contrast (signature$^{\text{Pre}}$) images (Fig. 4b–d). The AUCs and other indicators for these radiomics signatures are shown in Table 3.

Predictive Performance of the Individualized Nomogram

The heatmap revealing the correlation between clinical factors and the fused radiomic features is shown in Fig. 5a and b. When clinical and qualitative imaging factors were combined with signature$^{\text{pre+AP+PP}}$, there was no significant improvement in predictive performance (P = 0.307 in the training cohort and 0.128 in the external validation cohort; Supplemental Table 3).

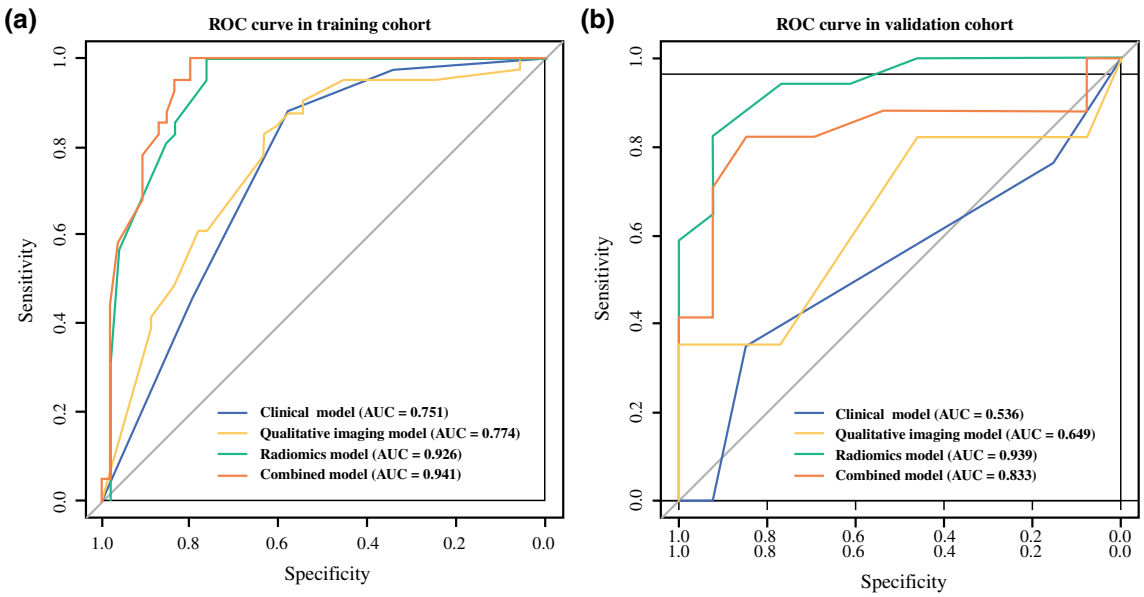

FIG. 3 **a** ROC curves for the clinical, qualitative imaging, radiomics, and combined models in the training cohort. **b** ROC curves for the clinical, qualitative imaging, radiomics, and combined models in the external validation cohort

The nomogram that was constructed based on the radiomics signature and related clinical factors is shown in Fig. 6a. The C-index of the nomogram in the training cohort was 0.941. However, the nomogram did not perform as well in the validation cohort (C-index = 0.833). The calibration curves for the training and external validation cohorts are shown in Fig. 6b and c. The predicted HGP status was in concordance with the actual HGP status (P = 0.990 in the training cohort and 0.089 in the external validation cohort).

DISCUSSION

In this study, radiomics signatures derived from contrast-enhanced MDCT were successful in distinguishing between desmoplastic and replacement HGPs of CRLMs. These results suggest that radiomics analysis based on MDCT images may serve as a useful noninvasive tool to predict HGP in patients with CRLMs.

Based on the previous study about the association between imaging and histopathological features, clear TLI and enhanced rim on MDCT post-contrast would be the major feature of desmoplastic HGP of CRLMs, which might be induced by surrounding a rim of fibrous band with blood supply from various extent of angiogenesis.[1,24,30] In contrast, CRLMs with replacement HGP would appear the obscure TLI and without obviously enhanced rim on MDCT post-contrast, which may be caused by the infiltration of tumor cell along the sinusoidal blood vessels and peri-sinusoidal space.[5,10,22] Our study's results supported these observations, as more desmoplastic HGP lesions demonstrated rim enhancement and clear TLI than did replacement HGP lesions on AP and PP images. The qualitative imaging model derived by integrating tumor size and location, TLI, and enhanced rim on AP and PP images demonstrated 71.9% accuracy in the training dataset but only 66.7% accuracy in the external validation dataset. These results highlight the challenges involved in determining HGP type, because it can be difficult for radiologists to visually detect the small and imperceptible differences contributed by the microvasculature on the interface between the tumor and liver parenchyma of CRLMs.

In this study, the fused radiomics signature$^{pre+AP+PP}$ (AUC of 0.926 and 0.939 in training and external validation cohort) showed the best ability to predict desmoplastic and replacement HGPs compared with qualitative imaging, clinical factors. The signature $^{pre+AP+PP}$ was constructed using first-order statistics, second-order statistics, and high-order statistics on pre-contrast, AP and PP phase MDCT images. The histogram-based first-order statistics described small differences in rim enhancement between desmoplastic and replacement CRLMs that cannot be exactly and quantitatively identified visually. These differences are primarily due to variations between desmoplastic and replacement HGPs in angiogenesis and vessel co-option. The second-order and high-order statistics described spatial relationships between voxels with similar gray levels within a lesion, providing a measure of heterogeneity between liver metastases and the surrounding parenchyma.[31] The features derived from radiomics analysis

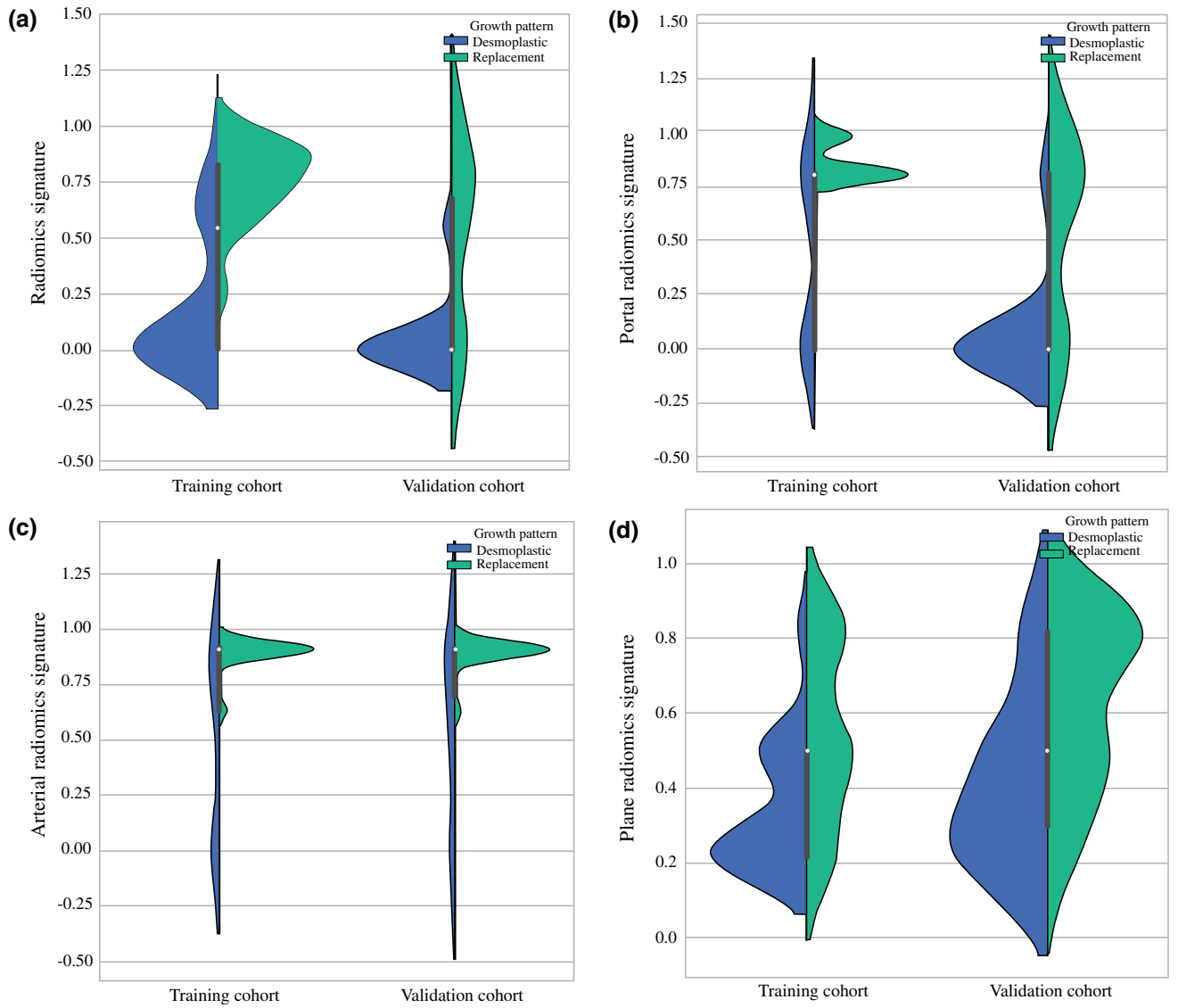

FIG. 4 **a** Violin graph of distribution of signature$^{pre+AP+PP}$ between replacement and desmoplastic HGPs. **b** Violin graph of distribution of signature^{PP} between replacement and desmoplastic HGPs. **c** Violin graph of distribution of signature^{AP} between replacement and desmoplastic HGPs. **d** Violin graph of distribution of signature^{pre} between replacement and desmoplastic HGPs

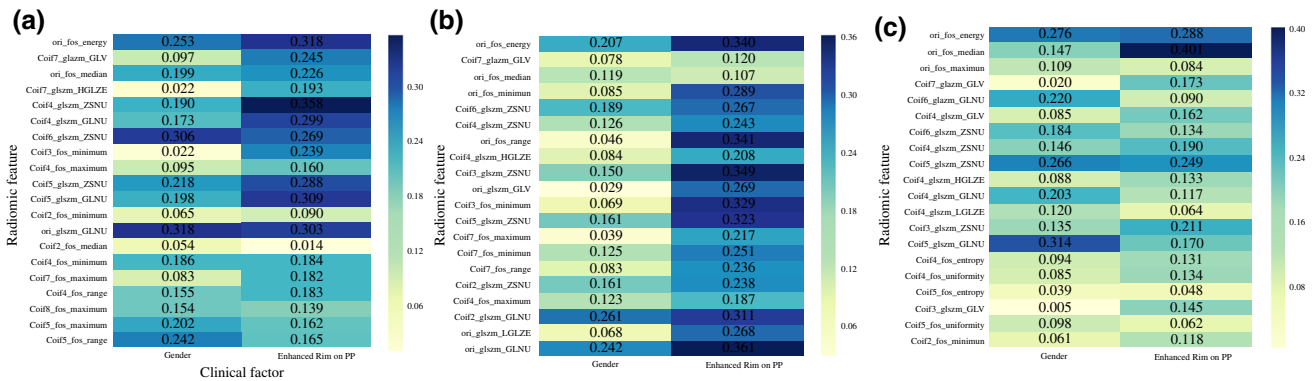

FIG. 5 **a** Heatmap demonstrating the correlation between clinical factors and postcontrast portal venous phase radiomic features. **b** Heatmap demonstrating the correlation between clinical factors and postcontrast arterial phase radiomic features. **c** Heatmap demonstrating the correlation between clinical factors and precontrast phase radiomic features

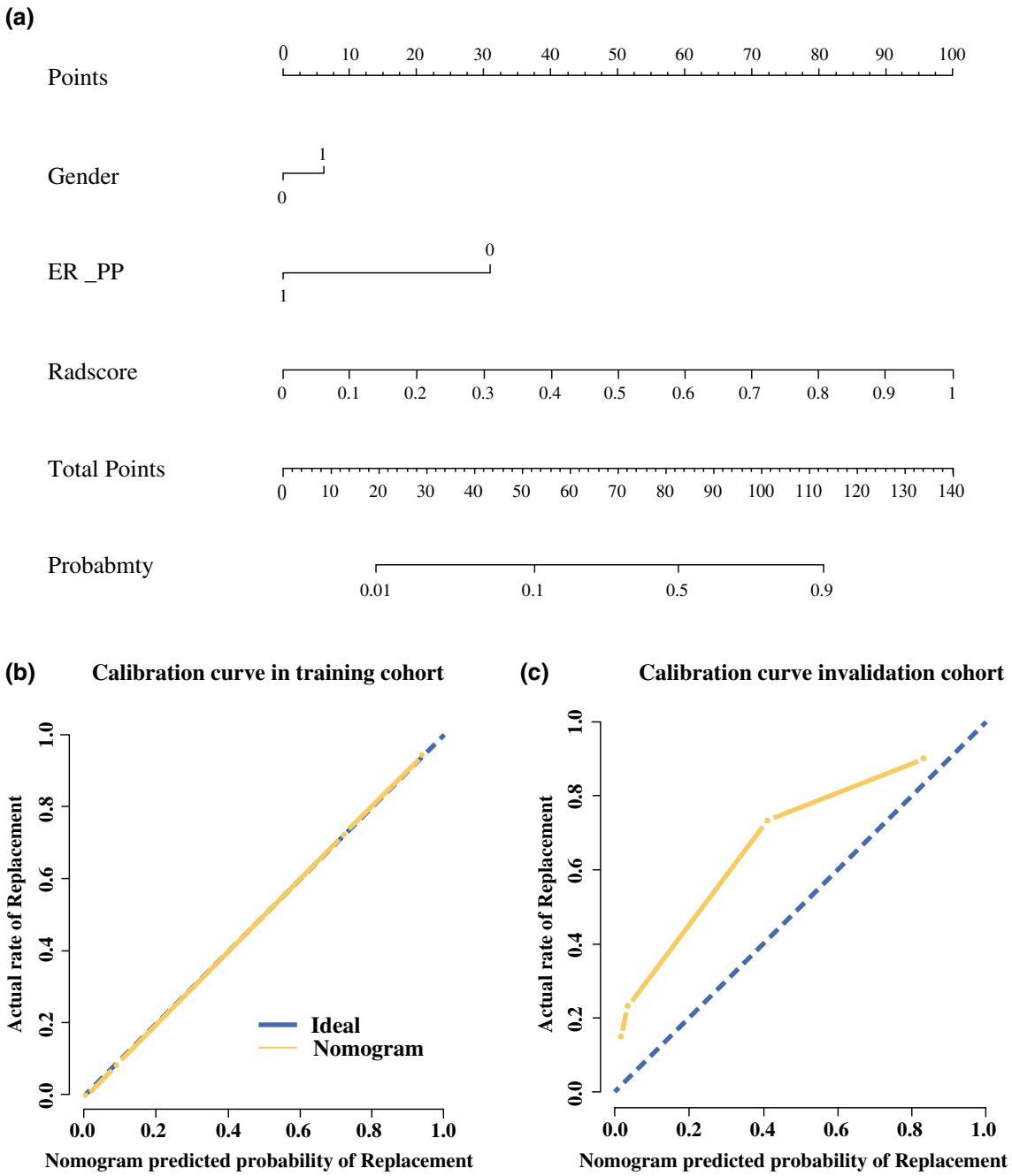

FIG. 6 **a** Nomogram constructed based on radiomics signature and related clinical factors. **b** Calibration curve of the nomogram in the training cohort. **c** Calibration curve of the nomogram in the external validation cohort

therefore yield important information that may help radiologists to better understand the phenotypes and microenvironment of these lesions.

There was no significant difference in the predicting performance between the radiomics model (constructed by the radiomics signature$^{pre+AP+PP}$) and the combined model (constructed by constructed by the radiomics signature$^{pre+AP+PP}$ with the clinical and the qualitative imaging factors). That means the addition of clinical and qualitative imaging factors to the predicting model did not significantly improve the model's accuracy.

Tumors in this study that were morphologically similar by visual inspection had large differences in quantitative parameters, highlighting the fact that radiomics analysis can be used to supplement radiologists' interpretations. This study also illustrates a link between standard MDCT images and tumor growth patterns and blood supply that may be induced by gene expression. A previous study

demonstrated that morphologic contrast enhancement imaging in glioblastomas was significantly associated with tumor angiogenesis.[32] Additionally, linear correlations have been demonstrated between CT texture heterogeneity features and the percentage of tumor angiogenesis.[16] In one prior study, tumor texture features were found to be associated with microvessel density, level of vascular endothelial growth factor, level soluble vascular endothelial growth factor receptor-1, and overall survival. Additionally, the mean value of positive pixels was found to be an independent prognostic factor in multivariate analysis.[33] To our knowledge, the current study is the first to show that radiomics analysis can be used to identify desmoplastic and replacement HGPs of CRLMs.

The heatmaps in this study demonstrated the degree of correlation between the extracted radiomic features and the enhanced rim on PP of each liver metastasis. This qualitative imaging feature might be induced by surrounding a rim of fibrous band with blood supply in the desmoplastic HGP.[1], [30] The contribution of sex to the combined predictive model could not be determined based on these initial results, which could be explained by the sample size as well as the inclusion of patients with multiple metastases possessing the same HGP. The C-index of the constructed nomogram of 0.941 in the training cohort and 0.833 in the external validation cohort, respectively. By using the nomogram, the probability of the CRLMs to be the replacement HGP will be got, which could be used as a potential reference of indicator selection before Bevacizumab-containing treatment.

This study was limited by its small sample size and retrospective design. Most patients with CRLMs are initially not suitable for resection, limiting the chemotherapy-naïve specimens available. For the same reasons, the survival analyses which might be influenced by the different HGPs of CRLMs was not included in this study. In the future study, we would make prospective design to investigate the survival difference between the patients who had liver metastases with different HGP. Only two patients had CRLMs with pushing HGP in this study; however, this result is in accordance with data published in the international consensus.[13] Despite the clear biological differences in HGP types, the molecular drivers of these differences are unknown. Mechanistic studies that elucidate these molecular drivers are therefore needed.

CONCLUSIONS

Our study suggests that a radiomics model derived from MDCT may effectively predict different HGPs of CRLMs, providing additional information for prognostic stratification and therapeutic decision-making. Although these results need to be validated in large-scale prospective studies, these initial findings suggest the potential for using radiomics analysis as a noninvasive biomarker for tumor phenotype.

ACKNOWLEDGMENT This work was supported by Natural Science Foundation of Beijing under Grant Nos. 7172226; Ministry of Science and Technology of China under Grant No. 2017YFA0205200; National Natural Science Foundation of China under Grant Nos. 81227901 and 81527805; Chinese Academy of Sciences under Grant Nos. GJJSTD20170004 and QYZDJ-SSW-JSC005; Beijing Municipal Science & Technology Commission under Grant Nos. Z161100002616022 and Z171100000117023; and the Key International Cooperation Projects of the Chinese Academy of Sciences under Grant No. 173211KYSB20160053.

DISCLOSURES The authors declare that they have no conflict of interest.

REFERENCES

1. Eefsen RL, Vermeulen PB, Christensen IJ, et al. Growth pattern of colorectal liver metastasis as a marker of recurrence risk. *Clin Exp Metastasis.* 2015;32(4):369–81.
2. Khatri VP, Chee KG, Petrelli NJ. Modern multimodality approach to hepatic colorectal metastases: solutions and controversies. *Surg Oncol.* 2007;16(1):71–83.
3. Hurwitz H, Fehrenbacher L, Novotny W, et al. Bevacizumab plus irinotecan, fluorouracil, and leucovorin for metastatic colorectal cancer. *N Engl J Med.* 2004;350(23):2335–42.
4. NCCN Clinical Practice Guidelines in Oncology (NCCN Guidelines®) Colon Cancer Version 3.2018. 2018; https://www.nccn.org/professionals/physician_gls/pdf/colon.pdf.
5. Vermeulen PB, Colpaert C, Salgado R, et al. Liver metastases from colorectal adenocarcinomas grow in three patterns with different angiogenesis and desmoplasia. *J Pathol.* 2001;195(3):336–42.
6. Van den Eynden GG, Bird NC, Majeed AW, Van Laere S, Dirix LY, Vermeulen PB. The histological growth pattern of colorectal cancer liver metastases has prognostic value. *Clin Exp Metastasis.* 2012;29(6):541–9.
7. Eefsen RL, Van den Eynden GG, Hoyer-Hansen G, et al. Histopathological growth pattern, proteolysis and angiogenesis in chemonaive patients resected for multiple colorectal liver metastases. *J Oncol.* 2012;2012:907971.
8. Paku S, Kopper L, Nagy P. Development of the vasculature in "pushing-type" liver metastases of an experimental colorectal cancer. *Int J Cancer.* Jul 20 2005;115(6):893–902.
9. Paku S, Lapis K. Morphological aspects of angiogenesis in experimental liver metastases. *Am J Pathol.* 1993;143(3):926–36.
10. Frentzas S, Simoneau E, Bridgeman VL, et al. Vessel co-option mediates resistance to anti-angiogenic therapy in liver metastases. *Nat Med.* 2016;22(11):1294–302.
11. Galjart B, Nierop PMH, van der Stok EP, et al. Angiogenic desmoplastic histopathological growth pattern as a prognostic marker of good outcome in patients with colorectal liver metastases. *Angiogenesis.* 2019;22(2):355–68.
12. Lazaris A, Amri A, Petrillo SK, et al. Vascularization of colorectal carcinoma liver metastasis: insight into stratification of patients for anti-angiogenic therapies. *J Pathol Clin Res.* 2018;4(3):184–92.

13. van Dam PJ, van der Stok EP, Teuwen LA, et al. International consensus guidelines for scoring the histopathological growth patterns of liver metastasis. *Br J Cancer.* 2017;117(10):1427–41.
14. Lambin P, Rios-Velazquez E, Leijenaar R, et al. Radiomics: extracting more information from medical images using advanced feature analysis. *Eur J Cancer.* 2012;48(4):441–6.
15. Sun R, Limkin EJ, Vakalopoulou M, et al. A radiomics approach to assess tumour-infiltrating CD8 cells and response to anti-PD-1 or anti-PD-L1 immunotherapy: an imaging biomarker, retrospective multicohort study. *Lancet Oncol.* 2018;19(9):1180–91.
16. Ganeshan B, Abaleke S, Young RC, Chatwin CR, Miles KA. Texture analysis of non-small cell lung cancer on unenhanced computed tomography: initial evidence for a relationship with tumour glucose metabolism and stage. *Cancer Imaging.* 2010;10:137–43.
17. Liu Z, Zhang XY, Shi YJ, et al. Radiomics analysis for evaluation of pathological complete response to neoadjuvant chemoradiotherapy in locally advanced rectal cancer. *Clin Cancer Res.* 2017;23(23): 7253–62.
18. Huang YQ, Liang CH, He L, et al. Development and validation of a radiomics nomogram for preoperative prediction of lymph node metastasis in colorectal cancer. *Sci Found China.* 2016;34(4): 2157–64.
19. Yang L, Dong D, Fang M, et al. Can CT-based radiomics signature predict KRAS/NRAS/BRAF mutations in colorectal cancer? *Eur Radiol.* 2018:1–10.
20. Van den Eynden GG, Majeed AW, Illemann M, et al. The multifaceted role of the microenvironment in liver metastasis: biology and clinical implications. *Cancer Res.* 2013;73(7): 2031–43.
21. Chun YS, Vauthey JN, Boonsirikamchai P, et al. Association of computed tomography morphologic criteria with pathologic response and survival in patients treated with bevacizumab for colorectal liver metastases. *JAMA.* 2009;302(21):2338–44.
22. Tirumani SH, Jagannathan JP, Braschi-Amirfarzan M, et al. Value of hepatocellular phase imaging after intravenous gadoxetate disodium for assessing hepatic metastases from gastroenteropancreatic neuroendocrine tumors: comparison with other MRI pulse sequences and with extracellular agent. *Abdom Radiol (NY).* Feb 22 2018.
23. Danet IM, Semelka RC, Leonardou P, et al. Spectrum of MRI appearances of untreated metastases of the liver. *AJR Am J Roentgenol.* 2003;181(3):809–17.
24. Inaba Y, Arai Y, Takeuchi Y, et al. [Enhancement pattern of hepatic metastases from colorectal cancer on CT arteriography]. *Nihon Igaku Hoshasen Gakkai Zasshi.* 1997;57(8):483–6.
25. Lunevicius R, Nakanishi H, Ito S, et al. Clinicopathological significance of fibrotic capsule formation around liver metastasis from colorectal cancer. *J Cancer Res Clin Oncol.* 2001; 127(3):193–9.
26. Sun H, Chen Y, Huang Q, et al. Psychoradiologic utility of MR imaging for diagnosis of attention deficit hyperactivity disorder: a radiomics analysis. *Radiology.* 2017;287(Suppl 11):170226.
27. Prasanna P, Patel J, Partovi S, Madabhushi A, Tiwari P. Radiomic features from the peritumoral brain parenchyma on treatment-naïve multi-parametric MR imaging predict long versus short-term survival in glioblastoma multiforme: preliminary findings. *Eur Radiol.* 2016;27(10):1–10.
28. Rios VE, Parmar C, Liu Y, et al. Somatic mutations drive distinct imaging phenotypes in lung cancer. *Cancer Res.* 2017;77(14):3922–30.
29. Kramer AA, Zimmerman JE. Assessing the calibration of mortality benchmarks in critical care: the Hosmer-Lemeshow test revisited. *Crit Care Med.* 2007;35(9):2052–6.
30. Semelka RC, Hussain SM, Marcos HB, Woosley JT. Perilesional enhancement of hepatic metastases: correlation between MR imaging and histopathologic findings-initial observations. *Radiology.* 2000;215(1):89–94.
31. Thibault G, Angulo J, Meyer F. Advanced statistical matrices for texture characterization: application to cell classification. *IEEE Trans Biomed Eng.* 2014;61(3):630–7.
32. Diehn M, Nardini C, Wang DS, et al. Identification of noninvasive imaging surrogates for brain tumor gene-expression modules. *Proc Natl Acad Sci USA.* 2008;105(13):5213–8.
33. Hayano K, Tian F, Kambadakone AR, et al. Texture analysis of non-contrast-enhanced computed tomography for assessing angiogenesis and survival of soft tissue sarcoma. *J Comput Assist Tomogr.* 2015;39(4):607–12.